Shaping the dynamics of a low-stiffness positioning system by mechatronic design for enabling stable unity gain feedback

Ernst Csencsics
Assistant Professor Measurement Systems
Automation and Control Institute
Technische Universität Wien
1040 Vienna, Austria
Email: csencsics@acin.tuwien.ac.at

Benjamin Friedl
Student assistant
Automation and Control Institute
Technische Universität Wien
1040 Vienna, Austria

Georg Schitter
Professor for Advanced Mechatronic Systems
Automation and Control Institute
Technische Universität Wien
1040 Vienna, Austria

This paper presents a method for enabling feedback control of a mechatronic system without a dedicated controller by tailoring structural modes of the mechanical structure for loop shaping by design. Structural modes are in general unwanted effects in positioning systems and are by design typically well separated from the frequency range over which control is effective. They can, however, also be deliberately integrated to shape the resulting loop gain of the control loop, to overcome the need for a dedicated position controller and enable unity gain feedback. The method employs a structural mode with anti-resonance-resonance-pattern together with a damping mechanism to obtain the required phase lead for feedback control of a low-stiffness positioning system. It is validated by an experimental setup with one degree of freedom, designed for a crossover frequency of 130 Hz and a phase margin of 50°. An adjustable electromagnetic damper is integrated to study the effects of parameter variations. The designed closed-loop controlled system achieves a bandwidth of 240 Hz, is capable of tracking step inputs and rejecting external impacts with settling times a factor 2 to 5 smaller than in the de-tuned case.

1 Introduction

A large number of industrial and scientific applications rely on the fast and precise positioning of objects, such as silicon wafers or measurement samples [1]. Particularly positioning systems in production plants and inline measuring devices are confronted with constantly growing demands on accuracy and speed [2]. Typical examples for systems integrating such positioning units include optical lithography machines for the semiconductor industry [3], [4], atomic force microscopes (AFMs) [5], [6], laser scanning microscopes [7], [8], optical 3D sensor systems [9], [10], or high-precision optical instruments [11]. In order to simplify the control of high-performance positioning systems, stiff designs are usually employed to avoid structural modes within or around the targeted control bandwidth. At the same time the desire for higher motion speeds, reduced energy consumption and minimizing costs demands ever lighter mechanical structures, that may no longer be considered as a rigid body in the relevant frequency range [12]. Additionally, increasing performance requirements need the bandwidth to increase, which may lead to the increased occurrence of structural modes within the system bandwidth and necessitates adapted control concepts [2], [13].

Next to advanced control concepts, also skillful design of the mechatronic components and in particular the mechanical structure can be used to handle these challenges. By deliberately integrating and shaping structural modes and dynamics the entire system performance can be advanced. They can for example be used to reduce the energy consumption of a positioning system by separating an initially rigid structure into two coupled subsystems with individual control needs [14]. Actively varied dynamics are also reported for an isolator with tunable electromagnetic mechanism to obtain high static and low dynamic stiffness [15]. Tuned mass dampers are another example for loop-shaping elements, which are used for improving the dynamics of scanning stages [16] and the performance of large space mirrors [17].

Post-print version of the article: E. Csencsics, B. Friedl, G. Schitter, "Shaping the Dynamics of a Low-Stiffness Positioning System by Mechatronic Design for Enabling Stable Unity Gain Feedback," *ASME Journal of Dynamic Systems, Measurement and Control*, vol. 145, no. 10, pp. 101001, 2023. DOI: 10.1115/1.4063074

The dynamic behavior of low-stiffness systems is usually dominated by the inertia of the moving masses. For feedback control a phase-lead generating component, e.g. a lead-lag element, is in general required to obtain a phase margin at the crossover frequency and ensure stability and robustness when closing the loop [18]. For describing all dynamic phenomena of the mechanics in servo positioning systems, including structural modes, in addition four patterns can be distinguished with respect to modal decomposition. The only pattern that generates the targeted lead-lag characteristic and the related phase lead is the combination of a second order zero (anti-resonance) followed by second order pole (resonance) [19]. The pattern is frequently encountered in mechatronic systems where several components are mounted to a mechanical mover frame as well as in the form of torsional and swaying modes of the mover, such as in CD-player pick-ups [1]. The simplest case can be found in the decoupling dynamics of a two-body system [12].

From a pure control perspective, the dynamics for shaping the loop gain can be implemented in any of the involved system components. This suggests that by an integrated design approach and loop shaping by design, the required phase lead for feedback control of a low-stiffness positioning system can be fully integrated into the mechatronic system structure by shaping a suitable structural mode with anti-resonance-resonance-pattern. With the potential advantage of enabling fully independent and feedback-controlled mechatronic units without dedicated controller for distributed systems or meta-materials, such as 3D printed or inflatable mechatronic structures [20, 21], this would clearly have the drawback of putting more effort on the design of the mechatronic system structure. However, a systematic method for such an integrated design of a positioning system with enabling stable unity gain feedback is not yet available.

The contribution of this paper is (i) a method for shaping the dynamics of a low-stiffness positioning system by mechatronic design to enable stable unity gain feedback and (ii) its experimental verification on a one degree-of-freedom (DoF) positioning system without dedicated feedback controller. Section 2 discusses typical controller dynamics together with their mechatronic analogies in the system structure. Based on the analogies, the loop shaping by design method is developed for tailoring the mechanical structure in order to obtain a desired loop gain in Section 3. The experimental setup is designed in Section 4, followed by the experimental validation of the designed system with mechatronically implemented feedback controller in Section 5. Section 6 concludes the paper.

2 Controller Dynamics and Mechatronic Analogies

From a control perspective, the loop gain, i.e. the product of plant and controller transfer function (TF), is determining the tracking and disturbance rejection performance of a system. It further enables the assessment of the closed-loop stability of the system in terms of gain and phase margins and is thus frequently used for the design of feedback controllers in a loop shaping approach [1]. For the typical control case with an already existing mechatronic positioning or scanning system, the controller is used to shape the resulting loop gain in order to obtain the desired bandwidth and stability margins or a transfer function tailored to a certain purpose [22]. However, as the loop gain results from the product of controller and plant, the desired dynamics can be integrated in either of the components. This means that in an integrated system design approach already the plant itself can be used to shape the resulting loop gain during the design phase of the mechatronic system [22].

Considering mechatronic systems with low or quasi-zero stiffness dynamics, which are typically controlled on their mass line, at least a phase-lead generating component, such as a lead-lag element, is needed to stabilize the system for feedback position control [18]. Typically, a constant gain is additionally required and an integrator improves low-frequency performance. Next to the position controller, a typical electromagnetically actuated low-stiffness system comprises amplifier electronics, a voice coil actuator, a mechanical structure including the mover, and a sensor to measure the current position. The desired dynamics can be implemented in either of the components or distributed over several of them. In the sense of an integrated system design, this requires to consider all system components and particularly their interplay from the very beginning of the design process.

For systems with low suspension modes or even zero and quasi-zero stiffness, the dynamics towards low frequencies are mainly determined by the moving mass, resembling a double (tamed) integrator in the frequency response. This means that for a freely floating mover a high loop gain towards low frequencies is already directly integrated and is determined by the effective mass of the designed mover.

A constant gain is simply a multiplicative factor and can be easily integrated by tailoring the power amplifier (PA), actuator (A) and/or position sensor (PS) gains accordingly. Depending on the mechanical structure of the system and within the limitations of maximum ratings, their product can be designed to result in the exact constant gain, locating the intersection of the mass line of the systems frequency response with the 0 dB-line at a desired crossover frequency.

Integrating a phase-lead generating element, which provides sufficient phase lead around a desired crossover frequency, into the mechatronic system is more challenging. It requires a mechanical analogy that results in a tunable lead-lag frequency response (tamed +20 dB/dec magnitude slope). With the desired phase lead and its spectral location, additionally two parameters have to be actively considered at the same time. In general, the targeted lead-lag dynamics and the related phase lead can be obtained from structural modes of the mechanical structure with an anti-resonance-resonance-pattern [19], as in the simplest case found in the typically undesired decoupling dynamics of a two-body system [12]. The dynamics of a two-body system with free-floating mover, as shown in Fig. 1, can be described by the transfer functions

Post-print version of the article: E. Csencsics, B. Friedl, G. Schitter, “Shaping the Dynamics of a Low-Stiffness Positioning System by Mechatronic Design for Enabling Stable Unity Gain Feedback,” *ASME Journal of Dynamic Systems, Measurement and Control*, vol. 145, no. 10, pp. 101001, 2023. DOI: 10.1115/1.4063074

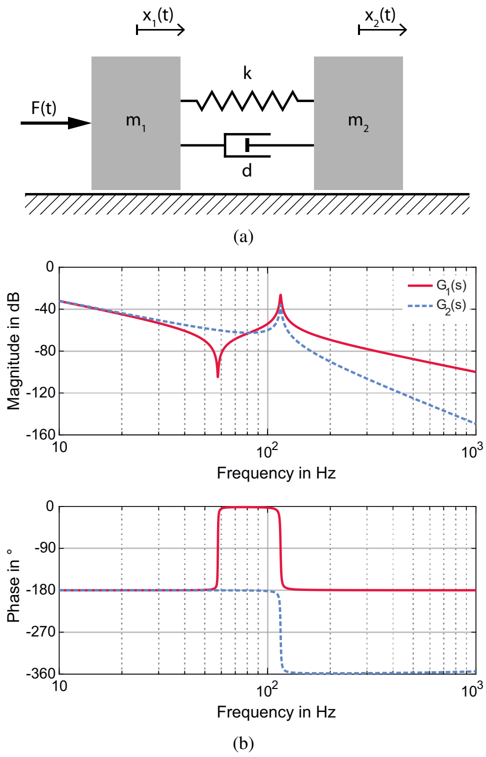

Fig. 1. Freely floating two-body system. (a) lumped mass model of the system. (b) the frequency response functions of the first, directly actuated body m_1 shows an anti-resonance and resonance pair around the decoupling frequency of the second body. The second body m_2 can no longer follow the motion of the first body after decoupling and shows a -80dB/dec. slope.

from input force to the position of the respective body

$$G_1(s) = \frac{X_1(s)}{F(s)} = \frac{m_2\, s^2 + d\, s + k}{m_1\, m_2\, s^4 + (m_1 + m_2)\,(d\, s + k)\, s^2}, \quad (1)$$

and

$$G_2(s) = \frac{X_2(s)}{F(s)} = \frac{d\, s + k}{m_1\, m_2\, s^4 + (m_1 + m_2)\,(d\, s + k)\, s^2}. \quad (2)$$

When the second body can no longer follow the motion of the directly actuated first body it decouples beyond a certain frequency (-80 dB/dec slope), as depicted in Fig. 1b. This decoupling entails an anti-resonance and a resonance in the dynamics of the actuated first body, resembling the desired lead-lag behavior with the required phase lead. Providing such a structural mode with anti-resonance-resonance-pattern with sufficient damping, the quality factors of the anti-resonance and resonance can be tuned together with the phase response for shaping the differential control action [23].

3 Loop Shaping via Mechanical Dynamics

In order to utilize the mechanical system dynamics for loop shaping in the design phase and enable unity gain feedback without a dedicated controller, the system with mechatronically integrated controller dynamics is modeled and parametrized. Without loss of generality, due to the modal decomposition method [1, 19], the following steps are performed for the structural mode with anti-resonance-resonance-pattern found in the decoupling dynamics of a two-body system. As only the the dynamics in the local frequency range around the crossover frequency are of importance, the method is also applicable to other structural modes. Systems with more complex mechanical structure and several structural modes, may require additional effort to obtain the following effective design parameters for a targeted system mode based on modal decomposition as well as to enable the integration of suitable damping mechanisms into the mechanical system structure.

3.1 Parametrized System Dynamics

Assuming that the position of the first, directly actuated mass m_1 of a two-body system is to be controlled, as shown in Fig. 1a, and that amplifier, actuator and position sensor are operated within their bandwidth and can thus be modeled by a combined constant gain K_G, the plant transfer function $G(s)$ from amplifier input $U(s)$ to measured position output $Y(s)$ is given by

$$\begin{aligned} G(s) &= \frac{Y(s)}{U(s)} = K_G\, G_1(s) \\ &= K_G \frac{m_2\, s^2 + d\, s + k}{m_1\, m_2\, s^4 + (m_1 + m_2)\,(d\, s + k)\, s^2}, \end{aligned} \quad (3)$$

By relating the physical system parameters to the mass m_1 using the design parameter set including the

$$\text{mass ratio } \mu = \frac{m_2}{m_1}, \quad (4a)$$

$$\text{specific damper constant } \delta = \frac{d}{m_1}, \quad (4b)$$

$$\text{specific spring constant } \kappa = \frac{k}{m_1}, \quad (4c)$$

$$\text{and specific gain } \rho = \frac{K_G}{m_1}, \quad (4d)$$

and considering that the amplifier input $U(s)$ directly equals the obtained position error of the first body $E(s)$ in the proposed configuration, as shown in Fig. 2, the loop gain transfer function $L(s)$ can be rewritten as

$$L(s) = \frac{Y(s)}{E(s)} = \frac{\rho}{s^2} \frac{\mu s^2 + \delta s + \kappa}{\mu s^2 + (1+\mu)\,(\delta s + \kappa)}. \quad (5)$$

The masses of the system no longer explicitly appear in the transfer function, such that all following calculations and results are independent of the actual mass of the system. The

Post-print version of the article: E. Csencsics, B. Friedl, G. Schitter, "Shaping the Dynamics of a Low-Stiffness Positioning System by Mechatronic Design for Enabling Stable Unity Gain Feedback," *ASME Journal of Dynamic Systems, Measurement and Control*, vol. 145, no. 10, pp. 101001, 2023. DOI: 10.1115/1.4063074

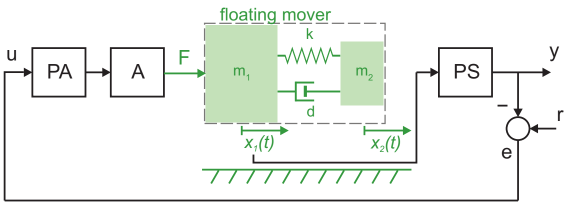

Fig. 2. Block diagram of a feedback-controlled system without dedicated controller. The loop shaping for stable feedback control of the position of m_1 is done by design and shaping the structural decoupling mode of the two-body system.

design parameters can be scaled to the real physical system by multiplying them with the designed mass m_1.

In order to assess stability and tracking performance of the position feedback control system for m_1, the Nyquist plot and criterion can be used. The system will become unstable upon closing the loop if the phase of the loop gain passes the negative real axis at an amplitude larger than one and does not return below the negative real axis before the gain gets smaller than one [1]. For a low-stiffness system without additional structural modes this essentially requires the loop gain in Eq. (5) to meet two conditions for stability [1] [24]:

- The magnitude $|L(j\omega)|$ intersects the 0 dB-line only once, namely at the crossover frequency ω_c.
- At the crossover frequency the phase lag $\arg L(j\omega)$ has to be less than 180°.

As can be seen in Fig. 1, the magnitude plot of the loop gain would cross the 0 dB-line up to three times when placing the crossover in the frequency range where the phase lead is largest. Incorporating sufficient damping, a strictly monotonically decreasing magnitude response can be achieved, while maintaining a phase margin of at least 50°, in order to add robustness to the system and keep the settling time and overshoot small [1] [18].

3.2 Design Method

The goal of the design method is to shape the phase lead between the anti-resonance and resonance to integrate the desired phase lead. For this purpose, the conditions for stability stated before are used to determine the parameters μ, δ, κ and ρ.

In the first step, the frequency ω_Φ at which the phase of the loop gain $L(s)$ becomes largest is determined by solving

$$\frac{\mathrm{d}}{\mathrm{d}\omega}\arg L(j\omega)\bigg|_{\omega=\omega_\Phi} = 0, \qquad (6)$$

which results in a sixth degree polynomial

$$\omega_\Phi^2\left(\omega_\Phi^4+\alpha\omega_\Phi^2+\beta\right)=0 \qquad (7)$$

with

$$\alpha = \frac{2+\mu}{\mu}\kappa - \frac{1+\mu}{\mu^2}\delta^2, \qquad (8a)$$

$$\beta = -3\frac{1+\mu}{\mu^2}\kappa^2. \qquad (8b)$$

Of the six solutions of Eq. (7), only the following one yields positive real values for ω_Φ.

$$\omega_\Phi = \sqrt{-\frac{\alpha}{2}+\sqrt{\frac{\alpha^2}{4}-\beta}}. \qquad (9)$$

Ideally, the maximum phase is placed at the desired crossover frequency ω_c. For the following calculations f_c = 130 Hz is chosen, which is also used for the experimental setup design in Section 4, such that

$$\omega_\Phi = \omega_c = 2\pi f_c \approx 817\,\mathrm{s}^{-1}. \qquad (10)$$

The numerically obtained solutions of Eq. (10) are shown as a function of the specific damper and spring constant δ and κ and for various mass ratios μ in Fig. 3a (solid lines). For every combination of κ and δ which lies above the curve belonging to the chosen mass ratio μ, the frequency with maximum phase ω_Φ will be larger than the crossover frequency ω_c. For points below the curve the opposite applies.

For the phase margin a minimum value of 50° is desired and under the assumption that Eq. (10) is fulfilled [1] the following relation is obtained

$$\Phi = 180^\circ + \arg L(j\omega_c)\big|_{\omega_c=\omega_\Phi} \geq \Phi_{min} = 50^\circ. \qquad (11)$$

The combinations of δ and κ where the phase margin equals Φ_{min} are for different mass ratios μ also shown in Fig. 3a (dashed lines). While all points above the related curve lead to a smaller phase margin than Φ_{min}, the points below will result in larger values. From these relations it follows that the parameter combination of δ and κ must be selected in the green shaded area to the right of the black dotted curve in Fig. 3a, which represents the intersections of the solid and dashed curves, in order to meet the requirements for the crossover frequency and the phase margin.

If the damping of the structural mode is too low, the magnitude of the loop gain has a positive slope around the phase lead between the anti-resonance and resonance (see Fig. 1). Since the maximum phase lead is placed at the desired crossover frequency, the magnitude would intersect the 0 dB-line three times. To ensure that the magnitude has a negative slope at the crossover frequency ω_c, where the maximum phase lead is placed (Eq. (10)), the condition

$$\Lambda = \frac{\mathrm{d}}{\mathrm{d}\omega}|L(j\omega)|\bigg|_{\omega=\omega_c=\omega_\Phi} < 0 \qquad (12)$$

Post-print version of the article: E. Csencsics, B. Friedl, G. Schitter, “Shaping the Dynamics of a Low-Stiffness Positioning System by Mechatronic Design for Enabling Stable Unity Gain Feedback,” *ASME Journal of Dynamic Systems, Measurement and Control*, vol. 145, no. 10, pp. 101001, 2023. DOI: 10.1115/1.4063074

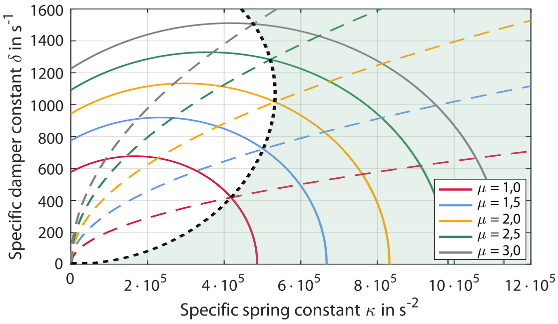

(a) Spectral location and value of the phase lead.

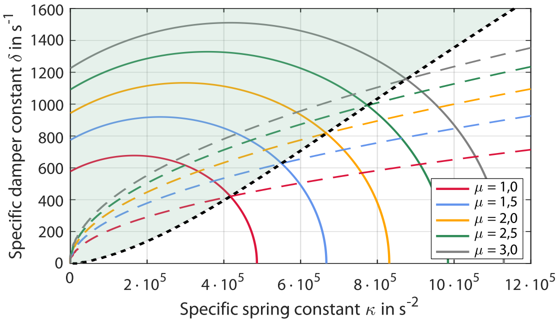

(b) Spectral location of the maximum phase lead and negative slope condition.

Fig. 3. Spectral locations of resulting phase lead and negative slope condition in the parameter space. Solid curves connect parameter combinations resulting in the same spectral location ω_Φ of the maximum phase lead (Eq. (10)). (a) Dashed curves connect combinations, resulting in the same phase lead value Φ_{min} (Eq. (11)). (b) Dashed curves connect combinations resulting in a zero magnitude slope at unity crossover. The green shaded areas mark respectively admissible parameter combinations.

is demanded. The dashed curves in Fig. 3b represent the points where the slope Λ is exactly zero. In order to obtain a negative slope, the selected parameter combination has to be located above the respective curve. As consequence, only parameter combinations in the green shaded area to the left of the black dotted curve satisfy Eqs. (10) and (12).

The two dotted lines from Fig. 3a and b define the admissible range for the selection of parameter combinations of δ and κ. Only if parameter combinations are chosen from the green shaded area in Fig. 4, the phase margin Φ will be above the minimum value and the slope of the magnitude Λ will be negative around the crossover. The further the selected combination is away from one of the limits, the larger is the margin for fulfilling the related condition.

With a chosen combination of κ and δ and a targeted crossover frequency ω_c, the mass ratio μ must be chosen so that Eq. (10) is fulfilled. When choosing the parameters for designing an integrated system, it must be taken into account that a larger mass ratio will result in a bigger total mass and therefore require a more powerful actuator and amplifier. A smaller mass ratio on the other hand increases the demand on the manufacturing tolerances of the mechanical system components and parameters, as the margins for acceptable parameter variations, which still lead to the targeted performance, decrease (see Fig. 4). Finally, the required design parameter ρ is calculated by rearranging the equation $|L(j\omega_c)| = 1$, resulting in

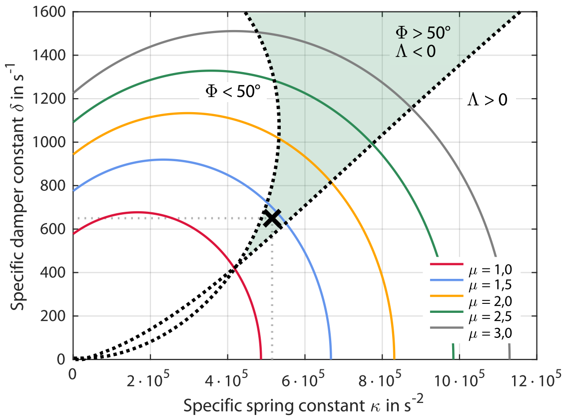

Fig. 4. Admissible parameter combinations. Parameter combinations in the green shaded area result in a phase margin lager than the minimum and a monotonically decreasing magnitude slope. The black cross marks the selected parameter combination for the experimental setup.

$$\rho = \omega_c^2 \sqrt{\frac{((1+\mu)\,\kappa - \mu\omega_c^2)^2 + ((1+\mu)\,\delta\omega_c)^2}{(\kappa - \mu\omega_c^2)^2 + (\delta\omega_c)^2}}. \qquad (13)$$

The design method can be applied to structural modes with anti-resonance-resonance-pattern in general. The parameters of a suitable structural mode can first be identified based on the modal decomposition method. The modified parameters that fulfill the stability requirements are then derived based on the proposed method, which is summarized in the following algorithm:

Algorithm 1 Algorithm for shaping the loop gain

Input: f_c, Φ_{min}, and m_1
Output: μ, δ, κ , and ρ
1: Evaluate (10) for feasible values μ (solid lines in Fig. 3)
2: Evaluate (11) to obtain parameter combinations with $\Phi \geq \Phi_{min}$ (green region in Fig. 3a)
3: Evaluate (12) to obtain parameter combinations with slope $\Lambda < 0$ at f_c (green region in Fig. 3b)
4: Chose combination of feasible κ and δ from the overlap region (green region in Fig. 4)
5: Identify related μ by solving (9)
6: Evaluate (13) to obtain $\rho = \rho(f_c, \mu, \kappa, \delta)$
7: **return** $\mu, \delta, \kappa, \rho$

Post-print version of the article: E. Csencsics, B. Friedl, G. Schitter, "Shaping the Dynamics of a Low-Stiffness Positioning System by Mechatronic Design for Enabling Stable Unity Gain Feedback," *ASME Journal of Dynamic Systems, Measurement and Control*, vol. 145, no. 10, pp. 101001, 2023. DOI: 10.1115/1.4063074

4 Experimental Positioning System with Integrated Control Dynamics

For the experimental setup a light-weight and robustly stable positioning system with one degree of freedom (DoF) is designed for a crossover frequency $f_c = 130\,\text{Hz}$, a phase margin $\Phi_{min} = 50°$ and a mass of the first body $m_1 = 0.33\,\text{kg}$. The chosen combination of design parameters together with the corresponding physical values for the mass m_1 are given in Table 1 and are also depicted in Fig. 4 (black cross). Figure 5 shows an image of the experimental setup. The basic structures of the two bodies (black parts) are 3D printed from *PETG* (polyethylene terephthalate glycol-modified) and are mounted on carriages with ball bearings, which move along a linear guide. The first body (m_1) is actuated by a voice coil actuator (*VCAR 0087-0062-00A*, *Suzhou Unite Precision Technology Co. Ltd., Suzhou, China*), which is driven by a current source with a bandwidth of 10 kHz. The position of the first body is measured by a Fabry-Perot interferometer (*M12/F0*, *attocube systems AG, Haar, Germany*) for which a small mirror is attached. The interface of the sensor provides an analogue output, which maps the measuring range of $\pm 1\,\text{mm}$ to $\pm 0.75\,\text{V}$, resulting in a sensor gain of $750\,\text{V/m}$.

Table 1. Selected specific and the corresponding real values.

Specific parameter	Value	Real parameter	Value
μ	1.44	m_2	0.48 kg
δ	$650\,\text{s}^{-1}$	d	215 kg/s
κ	$515 \times 10^3\,\text{s}^{-2}$	k	170 kN/m
ρ	$1.28 \times 10^6\,\text{s}^{-2}$	K_G	422 kN/m

The two bodies are connected via a rectangular leaf spring made from steel and an electromagnetic damper, which essentially represents the second body and is described in detail in Section 4.1. The two ends of the rectangular leaf spring are clamped to the second body, while its centre is mounted to the first body. Accordingly, the spring is modeled as two parallel bending beams with a total spring constant

$$k = 2\frac{F}{\Delta x} = \frac{bh^3}{2l^3}E = 159\,\text{kN/m}, \tag{14}$$

where $E = 210\,\text{GPa}$ is the Young's modulus and $l = 10\,\text{mm}$, $h = 0.6\,\text{mm}$ as well as $b = 7\,\text{mm}$ denote the distance between the clamping points, the thickness and the width of the steel sheet, respectively [25]. The summing point in Fig. 1a is realized as a custom-made differential amplifier with potentiometers, which also enables a fine adjustment of the resulting plant gain K_G [1].

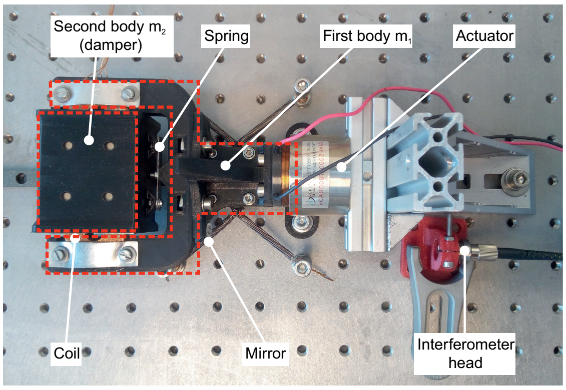

Fig. 5. Image of the experimental setup. The first body is actuated by a voice coil actuator along a linear guide and is connected to the second body via a leaf spring and an electromagnetic damper. The position of the first body is measured by an interferometer. To prevent the first body from drifting, it is suspended by four spiral springs with low stiffness.

4.1 Electromagnetic Damper Design

Since the damping is crucial for the stability of the control loop, the damper should show linear behavior and should be easily tunable to also investigate parameter variations. Thus, an electromagnetic damper based on the Lorentz force is designed and combined with a negative impedance converter (NIC; OPA544, Texas Instruments, Dallas, USA) to reduced the overall circuit impedance and increase the damping. Both components are schematically depicted in Fig. 6.

The permanent magnets (NdFeB, flux density = 1.22 T) generate a magnetic flux that is guided by steel sheets at the top and bottom of the assembly. Between the magnets are two coils with a total of N turns, which encompass the flux [26]

$$\Phi_v = NBa\left((c-x)-(c+x)\right) = -2NBax. \tag{15}$$

If the magnets and the coil are moved relative to each other with the velocity $v = \dot{x}$, a voltage is induced along the closed circuit path according to Faraday's law of induction

$$U = -\dot{\Phi}_v = 2NBav = (Z_S + Z_n)\,I \tag{16}$$

which entails a related current I determined via the coil impedance Z_S and the impedance of the NIC Z_n. As the current I flows through the magnetic field a velocity dependent Lorentz force $\vec{F}$ opposing the movement and according to

$$\begin{aligned}\vec{F} &= I\int_{\mathscr{C}} d\vec{s}\times\vec{B}\\ &= NI\left(a\left(-\vec{e}_y\right)\times B\vec{e}_z + a\vec{e}_y\times B\left(-\vec{e}_z\right)\right)\\ &= -\frac{4N^2B^2a^2}{Z_S+Z_n}v\vec{e}_x\end{aligned} \tag{17}$$

Post-print version of the article: E. Csencsics, B. Friedl, G. Schitter, "Shaping the Dynamics of a Low-Stiffness Positioning System by Mechatronic Design for Enabling Stable Unity Gain Feedback," *ASME Journal of Dynamic Systems, Measurement and Control*, vol. 145, no. 10, pp. 101001, 2023. DOI: 10.1115/1.4063074

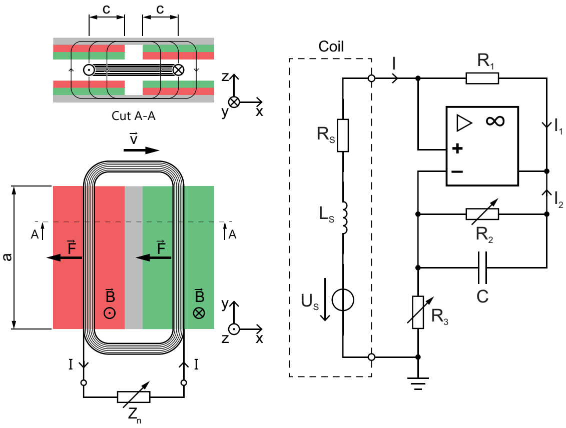

(a) Schematic of working principle.

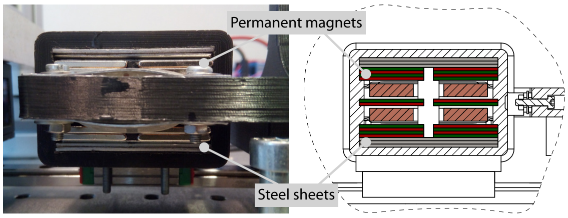

(b) Implemented damper.

Fig. 6. Tunable electromagnetic damper. (a) shows a schematic of the damper and the ngeative impedance converter circuit. When magnets and coil move relative to each other, a voltage is induced in the windings, which creates a current I that causes a damping force $\vec{F}$ opposing the movement. (b) depicts the implemented damper with permanent magnets and steel sheets as well as a schematic cross section.

is acting on the coil. Dividing the obtained force by the velocity, yields the damping coefficient

$$d = \frac{F}{v} = \frac{4N^2B^2a^2}{Z_S + Z_n} \tag{18}$$

of a linear damper model, which increases as the total impedance of the circuit in the denominator gets smaller.

The coil is modeled by an inductance L_S, a resistance R_S and an ideal voltage source U_S, which are connected in series, such that the coil impedance for a certain frequency ω is given by [27]

$$Z_S = R_S + j\omega L_S. \tag{19}$$

The NIC is used to reduce the overall impedance in the denominator of Eq. (18) and has an own impedance of [28]

$$Z_n = -\frac{R_1R_3}{R_2} - j\omega R_1R_3C. \tag{20}$$

Using these expressions in Eq. (18), yields

$$d = \frac{4N^2B^2a^2}{R_S - \dfrac{R_1R_3}{R_2}} \frac{1}{1 + \dfrac{\omega}{\omega_g}} \tag{21}$$

with

$$\omega_g = \frac{R_S - \dfrac{R_1R_3}{R_2}}{L_S - R_1R_3C}. \tag{22}$$

When using the NIC circuit, it must be ensured that both the real and the imaginary part of the total impedance $Z_S + Z_n$ are positive, as the circuit otherwise becomes unstable [28]. Since the current through the resistor R_1 is relatively large, it is realized as a ceramic resistor. The other two resistors R_2 and R_3 are potentiometers and used to tune the damping. From Eq. (21) the first order low pass behavior of the damper becomes evident. In order to obtain a constant damping within the frequency range of interest, a sufficiently high cut-off frequency ω_g (at least larger than the desired crossover frequency ω_c) has to be ensured when tuning the damper. For the components of the electrical circuit the values $R_1 = 10\,\Omega$, $R_2 = 2.78\,\mathrm{k}\Omega$, $R_3 = 2.03\,\mathrm{k}\Omega$ and $C = 470\,\mathrm{nF}$ were selected. This results in a cut-off frequency $\omega_g = 1613\,\mathrm{s}^{-1} \approx 2\,\omega_c$.

For the coils with 200 coil turns, self-supporting structures of 0.4 mm-thick insulated copper wire were used to keep the air gap of the magnetic circuit as small as possible. The resistance and inductance of the coil result to $R_S = 10.3\,\Omega$ and $L_S = 11.4\,\mathrm{mH}$, which were measured with a precision LCR meter (*E4980AL*, *Keysight Technologies, Santa Rosa, USA*).

4.2 Plant Identification

In order to identify the dynamic behavior of the experimental setup, a signal analyzer (*HP 3562A*, *Hewlett-Packard Company, Palo Alto, USA*) is used to measure the frequency response of the system from the input of the differential amplifier (second input grounded) to the output of the interferometer.

To investigate the sensitivity of the plant dynamics to parameter variations of the damper configuration in a first step, the loop gain is measured for varying values of the resistor R_3 in the NIC circuit, next to the tuned and undamped case. This affects the resulting damping value (see Eq. (21)) as depicted in Fig. 7. Already slight variations of the resistor of 5 and 10 % change the damping behavior significantly, turning the clean monotonically decreasing gain response of the tuned system configuration (dash-dotted red) into a response with clearly observable anti-resonance and resonance that entails three crossovers with the unity gain line. The phase response with lower damping shows sharper edges and an increased phase lead with almost 160° in the undamped case (solid blue), which is shifted to lower frequencies.

Post-print version of the article: E. Csencsics, B. Friedl, G. Schitter, "Shaping the Dynamics of a Low-Stiffness Positioning System by Mechatronic Design for Enabling Stable Unity Gain Feedback," *ASME Journal of Dynamic Systems, Measurement and Control*, vol. 145, no. 10, pp. 101001, 2023. DOI: 10.1115/1.4063074

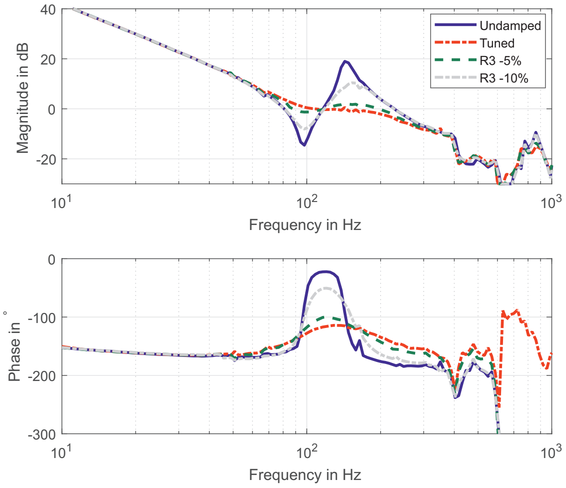

Fig. 7. Measured loop gain in dependence of the damping value. In the undamped case and with a 10 % smaller R_3 the conjugate complex pole and zero are clearly observable. The tuned case shows a monotonically decreasing gain response and a clean unity gain crossover with 50.1° phase margin.

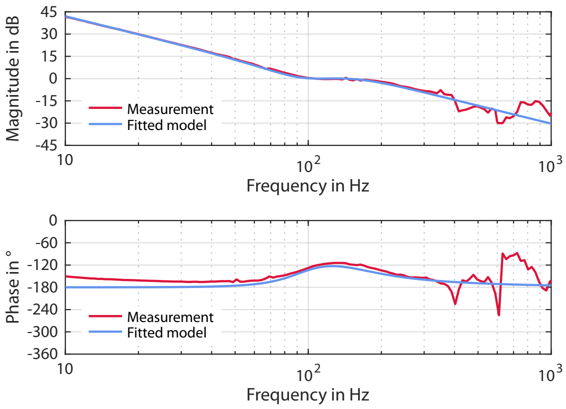

Fig. 8. Measured and modeled frequency response of the loop gain $L(s)$ with designed damper parameters. Due to the tailored damping of the structural dynamics there is only a single unity crossover.

The measured frequency response of the loop gain transfer function $L(s)$ with the properly tuned damper parameter values is again shown in Fig. 8 together with the fitted model. The anti-resonance and resonance are sufficiently damped such that the magnitude plot crosses the 0 dB-line only once at 139 Hz and there is a phase margin of 50.1° around the crossover frequency. Higher structural modes of the mover are observable beyond 400 Hz. The design parameters of the model according to Eq. (5) are fitted to the measured data and are given in Table 2 together with the related parameters of the physical system. The modeled transfer function based on these parameters shows good accordance with the measured frequency response. Due to simplifications of the model and manufacturing tolerances, the parameters slightly deviate from the target design parameter values. The increasing phase towards low frequencies can be explained by the fact that friction effects of the linear guiding become increasingly effective in this range.

Table 2. Fitted design parameters and the corresponding physical plant values.

Specific parameter	Value	Real parameter	Value
μ	1.4	m_2	0.46 kg
δ	560 s^{-1}	d	185 kg/s
κ	495×10^3 s^{-2}	k	163 kN/m
ρ	1.2×10^6 s^{-2}	K_G	396 kN/m

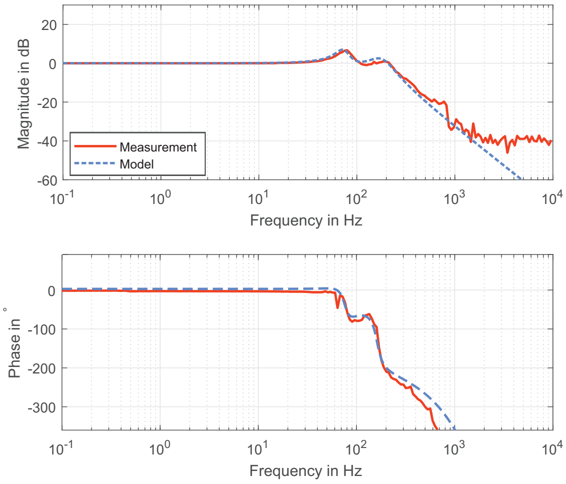

Fig. 9. Complementary sensitivity function with the designed damper parameters. The measured and modeled transfer functions show good agreement. The -3 dB bandwidth results to 240 Hz with a moderate gain peaking of 6.6 dB around 80 Hz.

5 Experimental Results

For investigating closed-loop behavior of the system, the complementary sensitivity function, the step response and the response to an impact or impulse are evaluated, together with the tracking error for an admissible raster trajectory.

The complementary sensitivity function is measured for the tuned damper case and compared to the modeled response in Fig. 9. Due to the comparably flat slope of the loop gain around the crossover, a slight double-peaking behavior is observed between 80 and 200 Hz. The 50° phase margin entails a moderate gain peaking of 6.6 dB around 80 Hz and the -3 dB bandwidth of system with mechatronically integrated controller results to 240 Hz. The measured response also shows good agreement with the modeled closed-loop frequency response.

From the step response in Fig. 10a it can be seen that a

Post-print version of the article: E. Csencsics, B. Friedl, G. Schitter, "Shaping the Dynamics of a Low-Stiffness Positioning System by Mechatronic Design for Enabling Stable Unity Gain Feedback," *ASME Journal of Dynamic Systems, Measurement and Control*, vol. 145, no. 10, pp. 101001, 2023. DOI: 10.1115/1.4063074

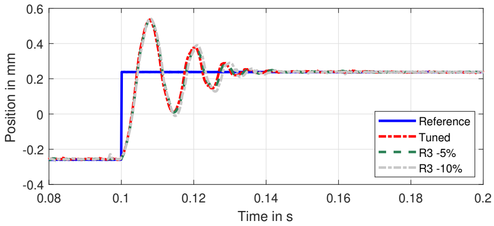

(a) Step response.

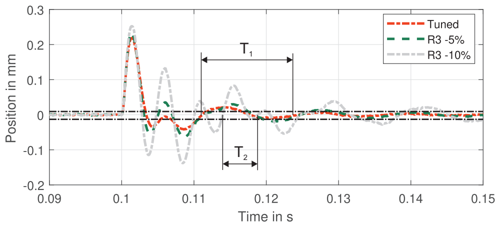

(b) Impulse Response.

Fig. 10. Tracking performance of feedback-controlled system. (a) shows the step response for varying damping values. (b) depicts the impulse response for varying damping values. The de-tuned configurations show increasingly higher oscillations after an impact and longer settling times to return to the 1% band (dash-dotted black).

variation of the damping value also affects the settling time of the feedback-controlled system. Reducing R_3 by 10 %, reduces the resulting damping value by about 20 % and leads to an increased settling time. In Fig. 10b the impulse response of the system with tuned and again slightly de-tuned damping parameters is depicted, which equals the case of a potential external impact onto the mover. The tuned system configuration compensates the impact well, showing quickly decreasing harmonic transients (period $T_1 = 0.0126$ s) with a frequency around the gain response peak at 80 Hz, as shown in Fig. 9. The configurations with increasingly detuned damping values show increasingly higher harmonic transients and longer settling times of 33.3 $\pm$ 1.1 ms (-5%) and 81.6 $\pm$ 1.3 ms (-10%) as compared to the settling time of the tuned case of 16.5 $\pm$ 0.7 ms (ten experiments per configuration). The peak transient values increase from 0.218 $\pm$ 0.002 mm for the tuned case to 0.233 $\pm$ 0.003 mm (-5%) and 0.257 $\pm$ 0.005 mm (-10%), respectively. The harmonic transients for the system with a 10 % smaller R_3 in addition have a significantly higher frequency of about 212 Hz (period $T_2 = 0.0046$ s), which is in the range of the third unity crossover frequency of the loop gain for this configuration (see Fig. 7). The phase margin amounts to only about 10° at this frequency, such that a large peak in the gain response of the complementary sensitivity function will result, explaining the frequency shift in the transient frequencies and demonstrating the importance of a properly tuned damping coefficient. In Fig. 11 the scanning performance of the system tracking a 10 Hz raster trajectory with an amplitude of 0.35 mm is depicted. Considering the crossover frequency of 139 Hz, thirteen higher harmonics of the 10 Hz triangle are covered by the system bandwidht, resulting in an rms tracking error of 7.8 μm, equal to 1% of the scan range, and a peak-to-valley error of 68 μm, which is mostly determined by the errors around the turning points.

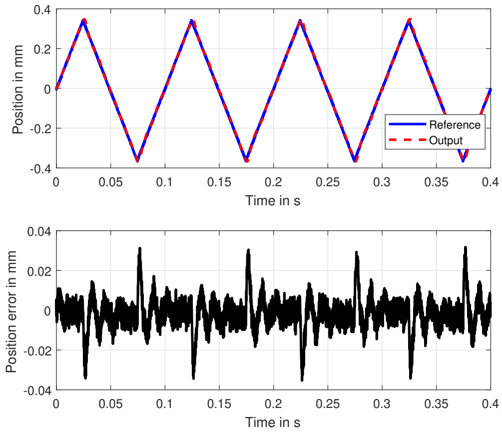

(a) Raster trajectory.

Fig. 11. Scanning performance of the feedback-controlled system tracking a 10 Hz raster trajectory together with the related error.

In summary, it is successfully shown that the proposed method enables loop shaping by design and position feedback control of a mechatronic low-stiffness system without a dedicated controller by using its mechanical structure to shape the loop gain and to generate the required phase lead.

6 Conclusion

In this paper a method for loop shaping by design, enabling feedback control of a mechatronic system without a dedicated controller by using its mechanical structure to shape the loop gain is developed. It is demonstrated that by utilizing mechanical dynamics of the mechatronic plant for loop shaping, the otherwise required control dynamics can be distributed over various system components. As consequence a dedicated feedback controller is no longer required. The developed method uses design parameters independent of the actual system mass, which makes it in principle applicable to systems of various size and structural dynamics with an anti-resonance-resonance pattern. The method is demonstrated by designing an experimental feedback controlled one DoF scanning system with decoupling dynamics for a targeted crossover frequency of 130 Hz and a phase margin of 50°. The experimental setup also integrates an adjustable electromagnetic damper, which is used to study the effects of damping variations on the resulting system performance. The closed-loop controlled system has a bandwidth of 240 Hz and is capable of tracking step inputs and rejecting external impacts with only minor transients.

Post-print version of the article: E. Csencsics, B. Friedl, G. Schitter, “Shaping the Dynamics of a Low-Stiffness Positioning System by Mechatronic Design for Enabling Stable Unity Gain Feedback,” *ASME Journal of Dynamic Systems, Measurement and Control*, vol. 145, no. 10, pp. 101001, 2023. DOI: 10.1115/1.4063074

Future work includes a generalization of this approach in combination with alternative passive damping mechanisms, such as tuned mass dampers, in order to enable the design of fully integrated feedback controlled distributed systems or meta-materials, such as 3D printed or inflatable mechatronic structures. While putting more design effort on the mechatronic system structure, this method could be an enabler for independent mechatronic units, which control performance can be tailored by tuning a single constant gain, e.g. in the form of a potentiometer.

References

[1] Schmidt, R. M., Schitter, G., Rankers, A., and van Eijk, J., 2014. *The Design of High Performance Mechatronics: High-Tech Functionality by Multidisciplinary System Integration*, 2nd revised edition ed. Delft University Press, Amsterdam.

[2] Oomen, T., 2018. "Advanced motion control for precision mechatronics: Control, identification, and learning of complex systems". *IEEJ Journal of Industry Applications,* **7**(2), pp. 127–140.

[3] Butler, H., 2011. "Position control in lithographic equipment". *IEEE Control Systems Magazine,* **31**(5).

[4] Schoot, J. V., van Ingen Schenau, K., Valentin, C., and Migura, S., 2015. "Euv lithography scanner for sub-8nm resolution.". *Extreme Ultraviolet (EUV) Lithography VI,* **9422**, p. 94221.

[5] Hansma, P., Schitter, G., Fantner, G., and Prater, C., 2006. "High speed atomic force microscopy". *Science,* **314**, pp. 601–602.

[6] Schitter, G., Astrom, K. J., DeMartini, B. E., Thurner, P. J., Turner, K. L., and Hansma, P. K., 2007. "Design and modeling of a high-speed afm-scanner". *IEEE Transactions on Control Systems Technology,* **15**(5), pp. 906–915.

[7] Gustafsson, M. G. L., 2000. "Surpassing the lateral resolution limit by a factor of two using structured illumination microscopy". *Journal of Microscopy,* **198**(2), pp. 82–87.

[8] Luca, G. M. D., Breedijk, R. M., Brandt, R. A., Zeelenberg, C. H., de Jong, B. E., Timmermans, W., and Manders, E. M., 2013. "Re-scan confocal microscopy: scanning twice for better resolution". *Biomedical optics express,* **4**(11), pp. 2644–2656.

[9] Schlarp, J., Csencsics, E., and Schitter, G., 2020. "Optical scanning of a laser triangulation sensor for 3d imaging". *IEEE Transactions on Instrumentation and Measurement,* **69**(6), pp. 3606–3613.

[10] Wertjanz, D., Kern, T., Csencsics, E., Stadler, G., and Schitter, G., 2021. "Compact scanning confocal chromatic sensor enabling precision 3-d measurements". *Applied Optics,* **60**(25), pp. 7511–7517.

[11] Yang, M., Zhang, C., Huang, X., Chen, S., and Yang, G., 2021. "A long-stroke nanopositioning stage with annular flexure guides". *IEEE/ASME Transactions on Mechatronics,* **27**(3), pp. 1570–1581.

[12] Csencsics, E., Thier, M., Hainisch, R., and Schitter, G., 2018. "System and control design of a voice coil actuated mechanically decoupling two-body vibration isolation system". *IEEE/ASME Transactions on Mechatronics,* **23**(1), pp. 321–330.

[13] Yuan, L., Chen, S., Zhang, C., and Yang, G., 2022. "Parameter space optimization for robust controller synthesis with structured feedback gain". *IEEE Transactions on Cybernetics*.

[14] Csencsics, E., Thier, M., Siegl, P., and Schitter, G., 2016. "Mechatronic design of an active two-body vibration isolation system". *Proceedings of the 7th IFAC Symposium on Mechatronic Systems,* **49**(21), pp. 133–140.

[15] Sun, Y., and et al., 2019. "High-static–low-dynamic stiffness isolator with tunable electromagnetic mechanism". *IEEE/ASME Transactions on Mechatronics,* **25**(1), pp. 316–326.

[16] Heertjes, M. F., van de Ven, M. L. J., and Kamidi, R., 2017. "Acceleration-snap feedforward scheme for a motion system withviscoelastic tuned-mass-damper". *American Control Conference*, pp. 2888–2893.

[17] Yingling, A. J., and Agrawal, B. N., 2014. "Applications of tuned mass dampers to improve performance of large space mirror". *Acta Astronautica,* **94**(1), pp. 1–13.

[18] Csencsics, E., and Schitter, G., 2017. "Parametric pid controller tuning for a fast steering mirror". *1st IEEE Conference on Control Technology and Applications, Kohala Coast, Hawaii, USA*.

[19] Rankers, A. M., 1997. "Machine dynamics in mechatronic systems - an engineering approach". PhD thesis, Twente University.

[20] Oliveira, J., Ferreira, A., and Reis, J. C. P., 2020. "Design and experiments on an inflatable link robot with a built-in vision sensor". *Mechatronics,* **65**, p. 102305.

[21] Chen, T., Pauly, M., and Reis, P. M., 2021. "A reprogrammable mechanical metamaterial with stable memory". *Nature,* **589**(7842), pp. 386–390.

[22] Csencsics, E., and Schitter, G., 2017. "System design and control of a resonant fast steering mirror for lissajous-based scanning". *IEEE/ASME Transactions on Mechatronics,* **22**(5), pp. 1963–1972.

[23] Csencsics, E., Thier, M., Hainisch, R., and Schitter, G., 2017. "System and control design of a voice coil actuated mechanically decoupling two-body vibration isolation system". *IEEE/ASME Transactions on Mechatronics,* **23**(1), pp. 321–330.

[24] Föllinger, O., and Dörrscheidt, F., 1994. *Regelungstechnik: Einführung in die Methoden und ihre Anwendung*, 8 ed. Hüthig, Heidelberg.

[25] Gross, D., Hauger, W., Schröder, J., and Wall, W. A., 2017. *Technische Mechanik 2*. Springer Berlin Heidelberg, Berlin, Heidelberg.

[26] Janssen, J. L. G., Paulides, J. J. H., Encica, L., and Lomonova, E., 2010. "High-performance moving-coil actuators with double-sided pm arrays: A design comparison". In 2010 International Conference on Electrical Machines and Systems, pp. 1657–1660.

Post-print version of the article: E. Csencsics, B. Friedl, G. Schitter, "Shaping the Dynamics of a Low-Stiffness Positioning System by Mechatronic Design for Enabling Stable Unity Gain Feedback," *ASME Journal of Dynamic Systems, Measurement and Control*, vol. 145, no. 10, pp. 101001, 2023. DOI: 10.1115/1.4063074

[27] Zhou, S., Jean-Mistral, C., and Chesné, S., 2019. "Electromagnetic shunt damping with negative impedances: Optimization and analysis". *Journal of Sound and Vibration,* **445**, pp. 188–203.

[28] Tietze, U., Schenk, C., and Gamm, E., 2016. *Halbleiter-Schaltungstechnik*, 15 ed. Springer Vieweg, Berlin and Heidelberg.

Post-print version of the article: E. Csencsics, B. Friedl, G. Schitter, "Shaping the Dynamics of a Low-Stiffness Positioning System by Mechatronic Design for Enabling Stable Unity Gain Feedback," *ASME Journal of Dynamic Systems, Measurement and Control*, vol. 145, no. 10, pp. 101001, 2023. DOI: 10.1115/1.4063074